Nanostructuring and stabilization of metastable rock-salt ZnO: impact of high-pressure media and compression geometry

Petr Sokolov, Alexandre Courac, Vladimir Solozhenko

Nanostructuring and stabilization of metastable rock-salt ZnO: Impact of high-pressure media and compression geometry

Petr S. Sokolov,[a] Alexandre Courac,[b,c] and Vladimir L. Solozhenko [a,*]

[a] *LSPM–CNRS, Université Sorbonne Paris Nord, 93430 Villetaneuse, France*

[b] *IMPMC, Sorbonne Université, UMR CNRS 7590, Muséum National d'Histoire Naturelle, IRD UMR 206, 75005 Paris, France*

[c] *Institut Universitaire de France (IUF), 75005 Paris, France*

Abstract. For complete and reproducible recovery of a high-pressure polymorph of zinc oxide, rock-salt ZnO (*rs*-ZnO), nanostructured wurtzite ZnO (*w*-ZnO) is typically used as a precursor for high-pressure synthesis. In the case of polycrystalline *w*-ZnO, only small amounts (less than 30 vol.%) of disordered/nanosized *rs*-ZnO were occasionally observed in the recovered products. Here we report the conditions for the synthesis of single-phase *rs*-ZnO from microcrystalline (40-50 μm) *w*-ZnO powder at 7.7 GPa and 2000 K. The complete recovery of metastable *rs*-ZnO is possible only by using a multianvil apparatus for quasi-hydrostatic (triaxial) compression/decompression and pyrolytic boron nitride as a pressure medium. Single-phase *rs*-ZnO was produced as colorless nanocrystalline well-sintered bulks with Vickers hardness up to 7 GPa - the record value for ZnO due to a fortunate combination of Hall-Petch nanostructuring effect and high intergranular purity. This unexpected phenomenon can be related to the mechanism of the direct and reverse phase transitions in ZnO, which requires "uniaxial" tensile deformation. Texture analysis of the recovered samples, as well as previous kinetic studies and *ab initio* simulation of strain-structure relationships, strongly support this model. Thus, 3-axial decompression is a more efficient tool – neglected until now – for reproducible recovery of high-pressure ZnO-based materials than the nature of the *w*-ZnO precursor and the presence of isostructural rock-salt phases.

Keywords: zinc oxide, high pressure, nanostructuring, phase stability, pressure medium

[*] Corresponding author (e-mail: vladimir.solozhenko@univ-paris13.fr)

Introduction

Extreme pressure-temperature conditions are a powerful tool for creating nanostructured materials.[1-7] Such materials are not only interesting for the fundamental understanding of microscopic phenomena due to nanostructuring (mechanical and transport properties, etc.), but also have great potential for advanced applications as wide bandgap semiconductors. In traditional experimental approaches, the recovery of high-pressure phases (diamond, stishovite, *rs*-ZnO, etc.) is linked to the time-pressure-temperature (*t*-*p*-*T*) synthesis protocol (e.g. rate of decompression/cooling from *p*-*T* synthesis conditions, decompression temperature, etc.) and the initial state of the precursors (e.g. grain size, impurities). For example, nanocrystalline stishovite (high-pressure polymorph of SiO_2) and *rs*-ZnO can be quenched down to ambient conditions starting from periodic mesoporous silica[3] and nanopowders of wurtzite ZnO,[4] respectively. The nanostructured *rs*-ZnO can be synthesized by using *w*-ZnO nanoparticles prepared either by solution chemistry[4] or by deep grinding in a ball mill.[8] Although this approach is quite successful, it has a number of limitations. The most crucial limitation is the purity of the starting nanopowders, which have high specific surface area and contain a large number of chemically bonded surface groups with possible stabilization effects (solution method) or mechanically introduced impurities (ball mill material in the case of deep grinding). This problem has been solved in the case of nanocrystalline diamond,[5] boron nitride,[6] and stishovite,[7] *i.e.*, in the cases where the phases can be easily recovered at ambient conditions, one only need to optimize the *t*-*p*-*T* conditions of direct solid-state phase transformations in order to ensure nanostructuring of a high-pressure phase. However, in the case of zinc oxide, this approach has not worked so far, and synthesis of pure *rs*-ZnO remains a major challenge, as does understanding of the properties of *rs*-ZnO-based materials (nanocomposites, solid solutions with transition metals, etc.).[9-10]

Zinc oxide is one of the most studied wide bandgap ionic semiconductors.[11] At ambient conditions, ZnO has a wurtzite structure ($P6_3mc$) that transforms into rock-salt one ($Fm3m$) at pressures above 5 GPa (the transition pressure p_{tr} is strongly dependent on temperature, grain size, etc., while equilibrium transition pressure p_{eq} is only weakly dependent on T).[8,12-19] Upon pressure release, as-synthesized *rs*-ZnO usually reverts back to wurtzite phase,[12] with significant hysteresis at temperatures below 1000 K. Occasionally, *rs*-ZnO can be recovered in the nanocrystalline state either in a mixture with *w*-ZnO or even in a pure form – in some special cases.[4,13] Recently, the recovery of the *rs*-ZnO has been intensively studied.[8,11-19] It was found that macroscopic (> 100 mm^3) nanocrystalline (grain size of 28-80 nm) samples of single-phase *rs*-ZnO can be recovered at ambient conditions from 7.7 GPa and 770-820 K when *w*-ZnO nanopowders with average grain size below 45 nm and narrow particle size distribution are used as precursors.[4,13-14] The recovery of *rs*-ZnO synthesized from ball-milled *w*-ZnO (grain size ~ 12 nm) at 15 GPa and 550 K in a diamond anvil cell (DAC) has also been reported.[8] However, the attempts to release pressure down to 0.1 GPa in a DAC indicated that *rs*-ZnO could be retained as a single phase for only ~10 min.[15] It was assumed that only well-crystallized

rs-ZnO could be recovered,[16] however, this hypothesis was later not confirmed.[4] Besides the nano-size of a precursor, the presence of isostructural compounds such as MgO[10] and NaCl[17] may also favor the recovery of synthesized *rs*-ZnO. At ambient pressure, thus recovered *rs*-ZnO/NaCl composites containing ~50 nm *rs*-ZnO particles are stable up to 360 K.[17] All this indicates a strong and unpredictable impact of kinetic factors related to the reversible transition of *w*-ZnO to *rs*-ZnO, which have been neglected so far in the analysis of the high-pressure phase recovery.

Here, we have developed a new approach for the complete recovery of single-phase *rs*-ZnO synthesized at high-pressure – high-temperature conditions from commercially available *w*-ZnO microcrystalline powders. We demonstrated that the sample environment (capsule of pyrolytic graphite-like BN) and the compression geometry (3-axial compression in a Walker-type multianvil (MA) high-pressure apparatus[20]) play an important role in phase stability of the resulting nanostructured *rs*-ZnO. To avoid the reverse transition, 3-axial decompression is an effective tool, as is the nature of the *w*-ZnO precursor[4] and the presence of isostructural compounds.[10],[17] The recovered bulk ingot of single phase *rs*-ZnO exhibits the highest hardness ever achieved for ZnO materials and the highest thermal stability – for the metastable rock-salt phase of ZnO.

Experimental

High-pressure synthesis of *rs*-ZnO was performed using a Walker-type multianvil apparatus,[20] which allows triaxial uniform compression of the high-pressure cell (pressure medium and sample). Conventional 14/8 high-pressure assemblies (Fig. 1a) were used. Microcrystalline powder of wurtzite ZnO (Alfa Aesar, 99.99%, -325 mesh) was placed in a capsule of pyrolytic hexagonal boron nitride hBN or MgO (sample volume ~ 3 mm^3), which served as a primary sample environment. The capsule was surrounded by a $LaCrO_3$ (or graphite) cylindrical resistive heater and placed in an octahedron of Cr_2O_3-doped MgO. Eight truncated tungsten carbide cubes (32 mm, 8-mm truncations, see Fig. 1a) served as the second stage anvils to compress the octahedron in three directions. Pressure and temperature were estimated using the "cell pressure *vs*. hydraulic oil pressure" and "cell temperature *vs*. supplied power" calibration curves, respectively. To construct the calibration curves, the direct *p*-*T* measurements were made using thermocouples (WRe5% - WRe26%, type C) and electrical resistivity changes in pressure standards (Bi, 2.55 and 7.7 GPa; PbSe, 4.2 GPa; PbTe, 5.2 GPa) at room temperature. In all cases, pressure and temperature uncertainties were estimated to be less than 0.5 GPa and 25 K, respectively. The high-pressure assembly was compressed to 7.7 GPa for 6 hours at room temperature, and then heated to 2000 K for 10 min. The sample was held at this temperature for one minute and quenched by turning off the power. Pressure was then slowly released for 15 hours and the sample was recovered.

A series of alternative quenching experiments at 7.7 GPa and ~2000 K were carried out using the high-temperature cell[21] of an opposite-anvil toroid-type high-pressure apparatus.[22] In this case, the compression geometry allows performing uniaxial compression with quite significant deviatoric.[13] The cell was pressure-calibrated at room temperature using phase transitions in Bi, PbSe and PbTe, and temperature-calibrated under pressure using well-established reference points: melting of Si, NaCl, CsCl, Pt, Rh, Al_2O_3, Mo and Ni–Mn–C ternary eutectic. The details are described elsewhere.[21] Samples were gradually compressed to 7.7 GPa, heated to the desired temperature for 5 minutes, then quenched by turning off the power and slowly decompressed. The typical time to apply and release pressure was about 10 minutes. Pressure and temperature uncertainties were estimated to be about 0.5 GPa and 30 K, respectively.

Thermal stability and thermal expansion of recovered *rs*-ZnO samples in the range of 300–1000 K at ambient pressure have been studied *in situ* by synchrotron powder X-ray diffraction at the B2 beamline of the DORIS III storage ring (HASYLAB, DESY).[23] Debye-Scherrer geometry with a rotating quartz capillary was used. The X-ray diffraction patterns were collected in the 2–70° 2θ-range ($\lambda = 0.69797$ Å) for 10 min in real time using the OBI image plate detector.[24] A NIST powder LaB_6 (Pm-3m, $a = 4.15695$ Å) was used as standard for detector calibration at 300 K. X-ray diffraction experiments were performed upon stepwise heating with a step of 50 K. Sample temperature was measured with a chromel-alumel thermocouple after stabilization for 5 minutes prior to each data acquisition.

Grain size and lattice strain of the recovered samples were calculated from the lines width of powder X-ray diffraction patterns using the Williamson-Hall method.[25] Direct observations of grain size were performed by transmission electron microscopy (TEM) using a JEOL 2011 microscope.

The homogeneity of the samples was tested by micro-Raman spectroscopy (mapping by 5-micron beam). Raman spectra were collected in the backscattering geometry using a Horiba Jobin Yvon HR800 spectrometer equipped with a 488 nm excitation laser.

The Vickers hardness was measured using a Struers Duramin-20 microhardness tester with indentation loads ranging from 0.1 to 20 N and a loading time of 10 s. Hard steel 421HV0.1 was used as a standard. A minimum of five indentations were made for each load to ensure reproducibility and homogeneity.

Results and Discussion

A number of recovery experiments have been performed with bulk microcrystalline powder of *w*-ZnO under similar pressure-temperature conditions *i.e.*, 7.7 GPa and 2000 K. Six representative experiments are described in Table 1. Three experiments (# 1, 2 and 3) were performed under triaxial compression in MA apparatus, and three others (# 4, 5 and 6) were performed under uniaxial compression in toroid-

type apparatus. Experiments # 1 and 4 were performed with capsules of well-sintered pyrolytic BN ceramic (Saint-Gobain, AX05 grade); # 2 and 5 with capsules of compressed hBN powder (technical grade powder provided by the Institute for Superhard Materials, Ukraine); and # 3 and 6 without capsules, i.e. in MgO sleeve and directly in graphite heater, respectively.

Uniaxial vs triaxial compression/decompression and sample environment. Fig. 2 shows the powder X-ray diffraction patterns of recovered samples # 1-6. Only in the case of pyrolytic hBN capsule and triaxial compression was it possible to recover pure *rs*-ZnO phase (# 1). Either uniaxial compression with the same capsule (# 4) or different sample environments with triaxial compression (# 2-3) do not show such an effect. It is also interesting to note that MgO (capsule of experiment # 3) does not affect the recovery even though it is isostructural to *rs*-ZnO and is known to stabilize *rs*-ZnO nanoparticles in the form of nanocomposite.[10,17] At this point it should be mentioned that neither cBN nor hBN are isostructural to *rs*-ZnO.

When capsules of compressed hBN powder were used, *rs*-ZnO was also observed in recovered samples after triaxial compression, but only as a by-product (~8 vol.%). In the case of uniaxial compression, the amount of *rs*-ZnO in the recovered products decreases from ~25 vol.% in the case of pyrolytic BN capsules to ~9 vol.% for capsules of compressed hBN powder. In the absence of a BN environment, both types of compression lead to pure *w*-ZnO phase: nanostructured in the case of toroid-type apparatus and microcrystalline in the case of multianvil device.

According to our previous observations in the experiments similar to #5 but at different temperatures,[4,12] the microcrystalline ZnO recovered from 7.7 GPa and ~800 K contained the traces (~3 vol.%) of *rs*-ZnO phase, while after increasing the synthesis temperature up to 1450-1650 K, no traces of *rs*-ZnO were detected.[13]

Exploring possible mechanisms. Thus, it can be concluded that both the triaxial compression and the BN environment favor the recovery of *rs*-ZnO. In the case of well sintered pyrolytic BN as the capsule material and the most uniform triaxial compression, 100% phase purity was achieved. Although a detailed understanding of such phenomena would require a systematic study of surface energies under extreme conditions, nucleation and growth mechanisms, as well as non-hydrostaticity and stress/strain/temperature distribution throughout the cell, some conclusions can be drawn from a simple comparison of results obtained for toroid-type and multianvil apparatuses. The main differences are as follows:

(1) High deviatoric strains and stresses in toroid-type apparatus during compression/decompression, and quenching.

(2) Pressure increase and release in the multianvil apparatus is very slow (6-15 hours) compared to the toroid-type apparatus (5-20 min).

(3) Quenching rate in the multianvil device (~600 K/s) is estimated to be higher than that in toroid-type apparatus (< 300 K/s), mainly due to the larger cell size of the latter.

(4) The pressure drop may also be different depending on the mechanical properties of the sample environment (*e.g*. different for compressed powders and sintered ceramics), as well as of the compression geometry (MA *vs*. toroid).

Due to the high-temperature conditions (intense diffusion processes in ZnO start above 1000 K),[13] in our experiments at 7.7 GPa and 2000 K, the as-formed *rs*-ZnO phase was usually microcrystalline, and hBN-to-cBN transformation was observed when BN capsules were used. However, in some cases, the formation of nanocrystalline *rs*-ZnO (isotropic particles ranging in size from 50 to 200 nm according to TEM; average grain size of ~60 nm according to powder X-ray diffraction data) was observed in recovered samples during the quenching/decompression stage. The recovered *w*-ZnO always has remarkably broader diffraction lines as compared to *rs*-ZnO (even if the reverse transition is not complete, see # 2 and 5 in Fig. 2). This is due to the fact, that *w*-ZnO is formed at much lower temperature/pressure during quenching/decompression.

In order to understand the results on the unexpected effect of BN on the recovery of *rs*-ZnO, we carried out a study on the chemical interaction between ZnO and BN under experimental conditions. In general, two possible interactions should be considered: mutual solubility and chemical reaction. The formation of solid solutions is solid solutions between cBN and hypothetical sphalerite (*F*-43*m*) ZnO is unlikely due to the large lattice size mismatch (a = 3.615 Å for cBN, and a = 4.563 Å for isostructural ZnO with ionic radii $r(Zn^{2+})$ = 0.60 Å; $r(O^{2-})$ = 1.38 Å in tetrahedral coordination).[26] The chemical reaction could lead to the formation of metallic Zn and boron oxide(s), similar to the interaction between elemental boron and ZnO (3.5 GPa and 1475 K).[27]

Chemical interaction between ZnO and BN (both in mixtures and at the capsule/sample contact surface) has been studied over a wide *p*-*T* range (4.2-7.7 GPa and 1500-2000 K) in recovery experiments in toroid-type apparatus. No solid-state interaction was observed on the timescale of a few hours.[28]

These results indicate that the stabilization of nanostructured rock-salt ZnO is not due to BN-ZnO interaction, which could influence the thermodynamics and kinetics (nucleation/growth) of the reverse transition to *w*-ZnO; but is mainly caused by mechanical aspects of compression/decompression and sample environment. Also, we should not neglect the time-scale impact and the extreme sensitivity of phase transition s in ZnO to the *p*-*T*-*time* history of the *w*-ZnO precursor,[13] especially due to thermally induced deactivation of nucleation sites, already at temperatures of ~400 K, and probably lower. In fact, the time scales of multianvil and toroid experiments are very different: 24 h (mainly due to slow compression/decompression) and 1-2 h (fast compression/decompression), respectively. The impact of the *p*-*time* history on the kinetics of phase transitions in ZnO has not been studied so far, but is likely to be very important. The faster compression/decompression introduces more defects into the material

and thus more nuclei for the phase transition. However, all these observations cannot be explained exclusively by the time scale phenomenon, as shown by parallel experiments in MA and toroid-type apparatuses; the compression conditions (deviatoric stresses and strains, etc.) are also important and influence the nucleation/growth processes on the hour scale. Theoretical simulations[29] and experimental observations[30] show that the uniaxial strain evolution may be intrinsic for direct *w*-ZnO → *rs*-ZnO and reverse *rs*-ZnO → *w*-ZnO transitions; thus, cold uniaxial decompression may additionally favor the *w*-ZnO nucleation and reverse transition in toroid experiments.

The above suggestions are supported by *ab initio* studies of the triaxial compression of *w*-ZnO (along [0001], [2-1-10] and [01-10] directions), its athermal transition to *rs*-ZnO and subsequent triaxial decompression of *rs*-ZnO to analyze the reversibility of the transition.[29] A decrease in pressure beyond the direct transition point will not result in a reverse transition. After triaxial decompression, metastable *rs*-ZnO remained kinetically stable. At the same time, the excess thermal energy may allow to overcome the energy barrier between two ZnO polymorphs, while in the experiment at ambient pressure, *rs*-ZnO has been observed well above 300 K. In the mentioned theoretical work, it has been suggested that defects (grain boundaries) can act as potential nucleation sites, but this effect has not been studied so far. During triaxial decompression, the reverse transition was predicted to occur only upon application of a small "negative" hydrostatic pressure (about -1 GPa). It is interesting to note that the strongest preferred orientation was observed for sample #6 (recovered nanocrystalline *w*-ZnO, complete reverse transition): the [11-20] and [10-10] directions were preferentially aligned along the compression axis of the toroid-type apparatus. In contrast, in other samples where *rs*-ZnO was observed (i.e., the reverse transition was partial), the observed preferred orientation was weak or even negligible. Thus, one can assume that uniaxial decompression in the toroid-type apparatus introduces more defects and energetically favorable nucleation sites in *rs*-ZnO, although it is not the only reason for the activation of the reverse transition. The purity and structural defects of the grain boundaries also play an important role. Thus, the axiality of decompression seems to be the most important factor in the recovery of *rs*-ZnO synthesized from commercial microcrystalline *w*-ZnO powder.

Finally, the major role in the recovery of *rs*-ZnO plays the underlying nucleation mechanism of the reverse transition, which implies non-uniform tensile strength along some crystallographic directions, in good agreement with *ab initio* predictions. Once the oversaturation becomes important (in the terms of pressure, p_{tr}-p_{eq} ~ -4 GPa for the reverse transition), the *rs*-ZnO → *w*-ZnO transition becomes possible and is often observed (at least partially).

Characterization of single-phase rs-ZnO. Pure *rs*-ZnO formed at 7.7 GPa and 2000 K in multianvil experiments (e.g. sample # 1) is shown in Fig. 1b. These *p*-*T* conditions allowed us to ensure the completeness of the *w*-ZnO → *rs*-ZnO phase transition[13,16] and to avoid ZnO melting.[28] The synchrotron powder X-ray diffraction pattern (Fig. 3a) has shown that the recovered sample is single phase with no trace of *w*-ZnO. Refinement of lattice parameters and phase composition was performed

using the structureless Le Bail profile analysis (FullProf software). The resulting lattice parameters were $a = 4.2771(6)$ Å for *rs*-ZnO and $a = 3.6195(7)$ Å for cBN, which are in good agreement with literature values.[4,8,12-16] The coherent scattering domains of *rs*-ZnO are of ~62(8) nm with a lattice strain of 0.28(2)% according to the Williamson-Hall method[25] (Fig. 3b), which is in good agreement with the TEM observations (Fig. 4a) of individual visible *rs*-ZnO grains (according to SAED, Fig. 4b), whose dimensions vary from 50 to 150 nm. It should be noted that long exposure of *rs*-ZnO grains to electron beam leads to reverse transition to *w*-ZnO.

The complete absence of the characteristic *w*-ZnO modes in the Raman spectra of sample # 1 is in perfect agreement with the X-ray diffraction data, providing additional evidence of phase purity; while surface mapping indicates the sample homogeneity.

At ambient pressure, the recovered metastable *rs*-ZnO (sample # 1) remains kinetically stable for at least six months (no further time evolution was studied), and upon heating undergoes a transition to *w*-ZnO only above 800 K, while nanocrystalline *rs*-ZnO previously synthesized from *w*-ZnO nanoparticles is kinetically stable only up to 360 K.[4,17,31] Such high thermal stability of *rs*-ZnO allows a refinement of its *p-V-T* equation of state (Fig. 5). The lattice parameter at ambient conditions agrees well with the extrapolation of previously reported high-pressure – high-temperature data,[32] and is most probably, related to a well-crystallized bulk *rs*-ZnO, in contrast to previous observations of a wide range of lattice parameters for nanocrystalline *rs*-ZnO depending on the synthesis method. The analytical expression for the *p-V-T* equation of state of the form

$$V(p,T) = \left[V(0,T)^{-\delta_T} + V(p,300)^{-\delta_T} - V(0,300)^{-\delta_T} \right]^{-1/\delta_T},$$[33]

with $V(0,T) = V(0,300)\,[1 + a\,(T\text{-}300) + b\,(T\text{-}300)^2]$ and $V(p,300) = V(0,300)\left(1 + B'_0\, p / B_0\right)^{-1/B_0}$, was used to fit the experimental data. The equation-of-state parameters were found to be $B_0 = 177$ GPa, $B_0' = 6.2$, $V_0 = 19.52$ cm^3/mol; $a = 4.2\times10^{-5}$, $b = 3.25\times10^{-9}$ and $\delta_T = 2.37$.

The Vickers hardness (H_V) of bulk single-phase nanocrystalline *rs*-ZnO (sample #1) is 7.0(15) GPa, while hardness of *rs*-ZnO synthesized from the solution-chemistry *w*-ZnO nanoparticles (quenched from 7.7 GPa and ~800 K)[4,12] is ~5.5(1.0) GPa (Fig. 6). The observed improvement of mechanical properties (over 25% in the case of H_V) is apparently due to the better sintering of the nanoparticles.

The measured hardness of single-crystal *w*-ZnO in (0001) direction is 3.7(0.5), and that of polycrystalline *w*-ZnO sintered at 4.2 GPa and 1000 K is in the range of 4.0-4.5 GPa. The theoretical hardness of *w*-ZnO is 4.8 GPa,[34] which is slightly higher than our experimental data, which can be explained on the one hand by the imperfect sintering of *w*-ZnO grains in polycrystals (confirmed by the tendency of H_V to decrease with applied force) and on the other hand by the hardness dependence on the crystallographic orientation. However, well sintered polycrystalline *w*-ZnO samples show values close to 5 GPa,[35] which is in good agreement with the H_V value calculated in the framework of the

thermodynamic model of hardness.[34] According to this model, for two compounds of the same chemical composition

$$\frac{H_2}{H_1} = \frac{N_1}{N_2}\frac{\rho_2}{\rho_1}$$

where ρ is a density and N is a coordination number. Considering that *rs*-ZnO is denser than *w*-ZnO, but has a higher coordination number (6 *vs.* 4), the hardness of *rs*-ZnO should be only 82% of that of *w*-ZnO, i.e. 3.9 GPa. The observed 5.5 and 7 GPa values can only be caused by the nanostructuring. The dramatic hardness increase in the case of nanostructured bulk *rs*-ZnO synthesized from commercial microcrystalline *w*-ZnO can thus be clearly attributed to the nano-size of the grains (Hall-Petch effect [36,37]) and the purity of the grain boundaries. A similar increase in hardness compared to single-crystal value has been observed in the case of nanocrystalline cBN obtained from bulk pyrolytic BN (+90%),[6] nanostructured diamond (+70%)[5], and nano-stishovite (+50%).[7]

Conclusions

Finally, we have shown that rock-salt ZnO can be completely recovered after high-pressure – high-temperature treatment of commercial microcrystalline *w*-ZnO in a multianvil press with pyrolytic BN sample environment at relatively low (7.7 GPa) pressure and high (~2000 K) temperature. The Vickers hardness of as-synthesized *rs*-ZnO is 7.0(1.5) GPa, which is the highest value ever reported for ZnO-based materials, achieved due to the fortunate combination of Hall-Petch nanostructuring effect and high intergrain purity. We have shown that the dense cubic ZnO polymorph is quenchable and remains kinetically stable up to 800 K (the highest temperature ever reported for *rs*-ZnO) and may be a promising for new applications. The results obtained indicate that not only the p-T-time conditions of synthesis and the grain size of the initial sample play an important role,[38] but also the compression geometry and the sample environment. The reported recoverability of rs-ZnO reveals more features and new possible routes for the stabilization of high-pressure polymorphs, being more complex than previously thought. According to our results, the axiality of decompression plays the major role in the recovery of *rs*-ZnO synthesized from microcrystalline *w*-ZnO: triaxial compression/decompression facilitates the recovery of the high-pressure phase. This result inspires the future exploration of the whole variety of available *w*-ZnO materials for recovery their analogues based on *rs*-ZnO. The described synthesis route may have significant implications not only for ZnO and other $A^{II}B^{VI}$ compounds, but also for general $A^{N}B^{8-N}$ materials (e.g., AlN).[39]

Acknowledgments

The authors thank T. Chauveau and A.M.T. Bell for help with X-ray diffraction experiments, O. Brinza for help with TEM studies and A.N. Baranov for fruitful discussions. P.S.S. is grateful to the "Science and Engineering for Advanced Materials and devices" (SEAM) Lab of Excellence for financial support. X-ray diffraction studies at B2 beamline (DORIS-III) were performed during the beamtime allocated to the Project DESY-D-I-20100021 EC at HASYLAB-DESY.

References

1. G. Demazeau, *C.R. Chimie*, 2009, **12**, 933-942.
2. R. C. Liebermann, *High Press. Res.*, 2011, **31**, 493-532.
3. P. Mohanty, D. Li, T. Liu, Y. Fei and K. Landskron, *J. Amer. Chem. Soc.*, 2009, **131**, 2764-2765.
4. A. N. Baranov, P. S. Sokolov, V. A. Tafeenko, C. Lathe, Y. V. Zubavichus, A. A. Veligzhanin, M. V. Chukichev and V. L. Solozhenko, *Chem. Mater.*, 2013, **25**, 1775-1782.
5. T. Irifune, A. Kurio, S. Sakamoto, T. Inoue and H. Sumiya, *Nature*, 2003, **421**, 599-600.
6. V. L. Solozhenko, O. O. Kurakevych and Y. Le Godec, *Adv. Mater.*, 2012, **24**, 1540-1544.
7. N. Nishiyama, S. Seike, T. Hamaguchi, T. Irifune, M. Matsushita, M. Takahashi, H. Ohfuji and Y. Kono, *Script. Mater.*, 2012, **67**, 955-958.
8. F. Decremps, J. Pellicer-Porres, F. Datchi, J. P. Itie, A. Polian, F. Baudelet and J. Z. Jiang, *Appl. Phys. Lett.*, 2002, **81**, 4820-4822.
9. A. N. Baranov, P. S. Sokolov, O. O. Kurakevych, V. A. Tafeenko, D. Trots and V. L. Solozhenko, *High Press. Res.*, 2008, **28**, 515-519.
10. A. N. Baranov, O. O. Kurakevych, V. A. Tafeenko, P. S. Sokolov, G. N. Panin and V. L. Solozhenko, *J. Appl. Phys.*, 2010, **107**, 073519.
11. C. Klingshirn, J. Fallert, H. Zhou, J. Sartor, C. Thiele, F. Maier-Flaig, D. Schneider and H. Kalt, *Phys. Stat. Solidi B*, 2010, **244**, 1424-1447.
12. A. Mujica, A. Rubio, A. Munoz and R. J. Needs, *Rev. Mod. Phys.*, 2003, **75**, 863-912.
13. V. L. Solozhenko, O. O. Kurakevych, P. S. Sokolov and A. N. Baranov, *J. Phys. Chem. A*, 2011, **115**, 4354-4358.
14. P. S. Sokolov, A. N. Baranov, A. M. T. Bell and V. L. Solozhenko, *Solid State Commun.*, 2013, **177**, 65-67.
15. A. A. Politov, B. A. Fursenko, I. Y. Prosanov, S. V. Mytnichenko and V. V. Boldyrev, *Doklady Akademii nauk SSSR*, 1994, **334**, 194-196.
16. K. Kusaba, Y. Syono and T. Kikegawa, *Proc. Japan Acad.*, 1999, **75(B)**, 1-6.
17. P. S. Sokolov, A. N. Baranov, Z. V. Dobrokhotova and V. L. Solozhenko, *Russ. Chem. Bull.*, 2010, **59**, 325-328.
18. L. Bayarjargal, L. Wiehl and B. Winkler, *High Press. Res.*, 2013, **33**, 642-651.

19. A. Duzynska, R. Hrubiak, V. Drozd, H. Teisseyre, Paszkowicz, A. W. Reszka, A. Kaminska, S. Saxena, J. D. Fidelus, J. Grabis, C. J. Monty and A. Suchocki, *High Press. Res.*, 2012, **32**, 354-363.

20. D. Walker, M. A. Carpenter and C. M. Hitch, *Amer. Mineral.*, 1990, **75**, 1020-1028.

21. V. A. Mukhanov, P. S. Sokolov and V. L. Solozhenko, *J. Superhard Mater.*, 2012, **34**, 211-213.

22. L. G. Khvostantsev, V. N. Slesarev and V. V. Brazhkin, *High Press. Res.*, 2004, **24**, 371-383.

23. M. Knapp, C. Baehtz, H. Ehrenberg and H. Fuess, *J. Synch. Rad.*, 2004, **11**, 328-334.

24. M. Knapp, V. Joco, C. Baehtz, H. H. Brecht, A. Berghäuser, H. Ehrenberg, H. von Seggern and H. Fuess, *Nucl. Instr. Meth. Phys. Res. A*, 2004, **521**, 565-570.

25. G. K. Williamson and W. H. Hall, *Acta Metall.*, 1953, **1**, 22-31.

26. R. D. Shannon, *Acta Crystallogr. A*, 1976, **32**, 751-767.

27. X. Liu, X. Zhao, W. Hou and W. Su, *J. Alloys Compd.*, 1995, **223**, L7-L9.

28. A. N. Baranov, P. S. Sokolov and V. L. Solozhenko, *Crystals*, 2022, **12**, 744.

29. A. J. Kulkarni, K. Sarasamak, J. Wang, F. J. Ke, S. Limpijumnong and M. Zhou, *Mechan. Res. Comm.*, 2008, **35**, 73-80.

30. X. Yan, H. Dong, Y. Li, C. Lin, C. Park, D. He and W. Yang, *Sci. Rep.*, 2016, **6**, 24958.

31. F. Y. Sharikov, P. S. Sokolov, A. N. Baranov and V. L. Solozhenko, *Mendeleev Commun.*, 2017, **27**, 613-614.

32. F. Decremps, J. Zhang and J. R. C. Liebermann, *Europhys. Lett.*, 2000, **51**, 268.

33. O. O. Kurakevych, Y. Le Godec, V. L. Solozhenko*, J. Phys. Conf. Ser.*, 2017, **950**, 042023.

34. V. A. Mukhanov, O. O. Kurakevych and V. L. Solozhenko, *J. Superhard Mater.*, 2008, **30**, 368-378.

35. I. Yonenaga, *Physica B*, 2001, **308-310**, 1150-1152.

36. E. O. Hall, *Proc. Phys. Soc. B,* 1951, **64**, 747-755.

37. N. J. Petch, *J. Iron Steel Inst.* 1953, **174**, 25-28.

38. W. H. Wang, W. Utsumi and X.-L. Wang, *Europhys. Lett.*, 2005, **71**, 611-617.

39. K. Keller, T. Schlothauer, M. Schwarz, G. Heidea and E. Kroke, *High Press. Res.*, 2012, **32**, 23-29.

Table 1. Experimental details of representative experiments at 7.7 GPa and 2000 K.

NN	Sample environment	HP apparatus	Phase composition of the recovered sample
#1	*w*-ZnO / BN ceramic	MA	*rs*-ZnO + cBN
#2	*w*-ZnO / hBN powder	MA	*w*-ZnO + *rs*-ZnO (traces) + cBN + hBN (traces)
#3	*w*-ZnO / MgO	MA	*w*-ZnO
#4	*w*-ZnO / BN ceramic	Toroid	*w*-ZnO + *rs*-ZnO (~25 vol.%) + cBN
#5	*w*-ZnO / hBN powder	Toroid	*w*-ZnO + *rs*-ZnO (traces) + cBN + hBN (traces)
#6	*w*-ZnO / graphite	Toroid	*w*-ZnO (preferred orientation)

Notes: Weight ratio of hBN and *w*-ZnO was 1:1 (#2 and #5).

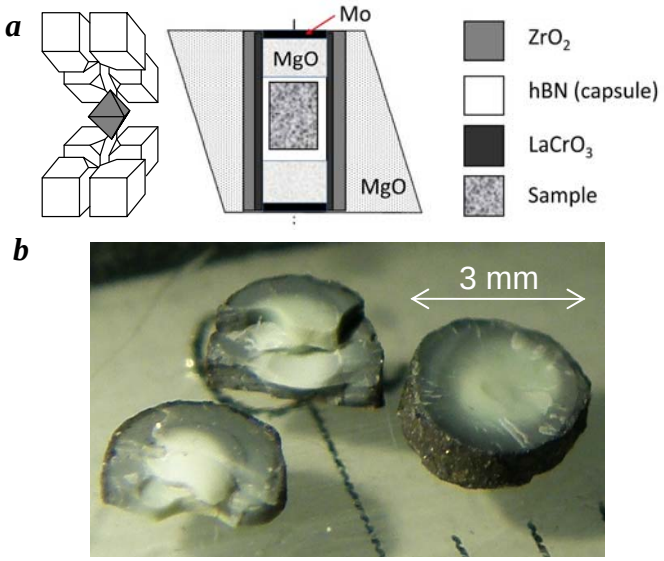

Figure 1 (*a*) Second stage of multianvil assembly (left) and high-pressure cell (right) used for synthesis. (*b*) Optical microscope image of *rs*-ZnO (white inner part) in cBN (grayish transformed pyrolytic hBN capsule) and $LaCrO_3$ heater (black outer part).

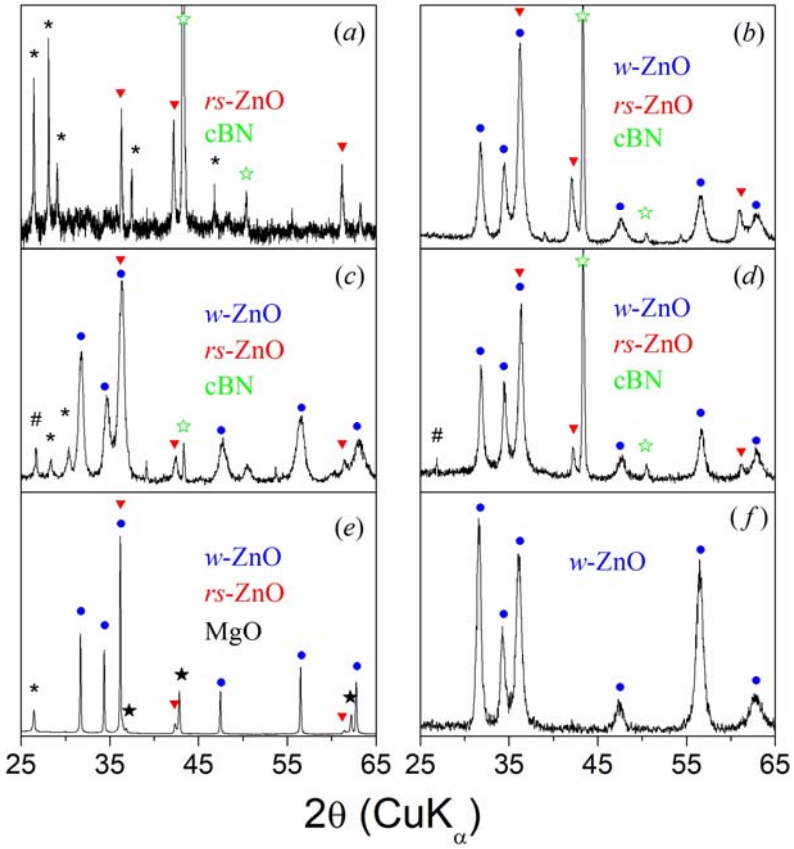

Figure 2 X-ray diffraction patterns of recovered ZnO samples: (a) # 1; (b) # 4; (c) # 2; (d) # 5; (e) # 3; (f) # 6. Sample # 1 is bulk, all other samples are fine powders. The # symbol indicates the 002 hBN line, and the * symbols correspond to the components of the high-pressure assembly.

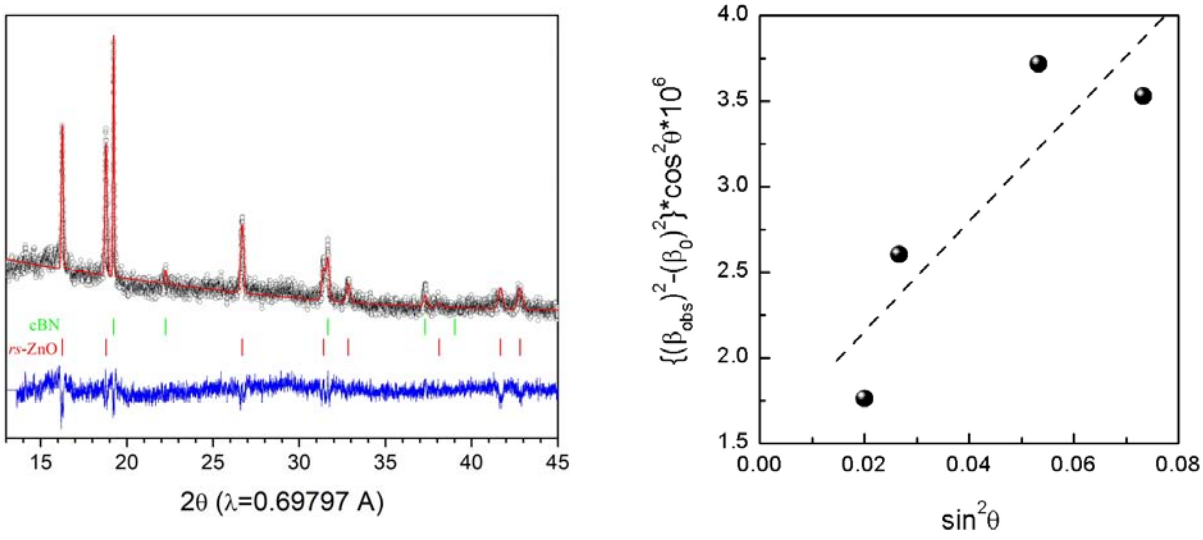

(*a*) (*b*)

Figure 3 (*a*) Experimental (circles), calculated (solid line) and difference (bottom) X-ray diffraction pattern (λ = 0.69797 Å) of the nanocrystalline *rs*-ZnO (sample # 1) quenched from 7.7 GPa and 2000 K. The pattern was collected at ambient pressure. Vertical bars indicate the Braggs peak positions for *rs*-ZnO and *c*BN (capsule material). (*b*) Williamson-Hall plot for sample # 1: β_{obs} – the integral width of *rs*-ZnO lines determined by fitting to the Gaussian profile function, β_0 – the integral width of LaB_6 (NIST standard) lines.

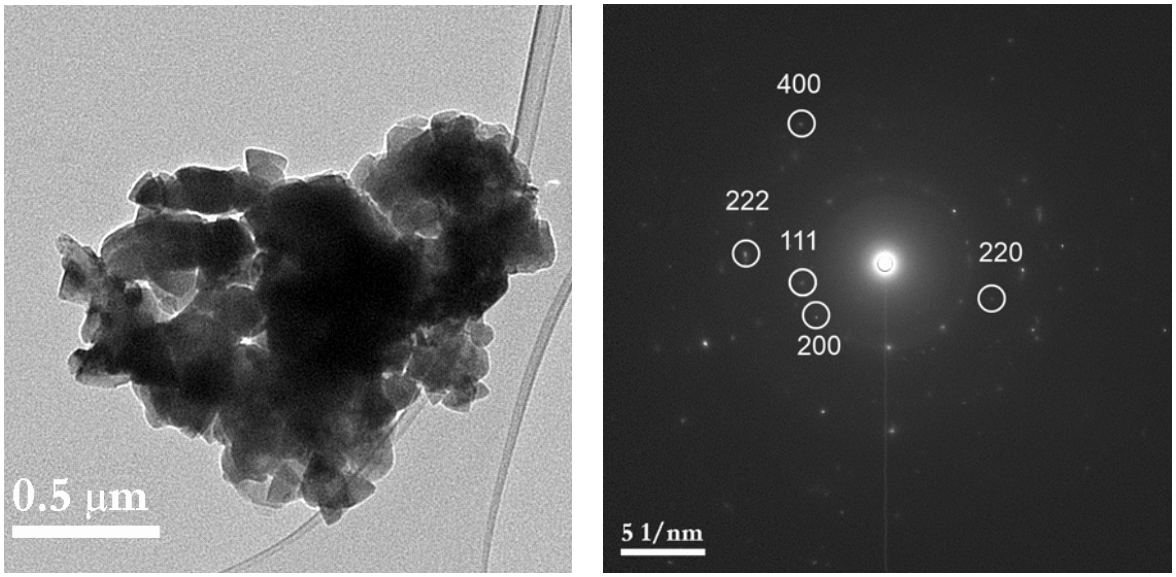

(*a*) (*b*)

Figure 4 (*a*) Transmission electron microscopy image and (*b*) selected area electron diffraction of nanocrystalline *rs*-ZnO (sample # 1).

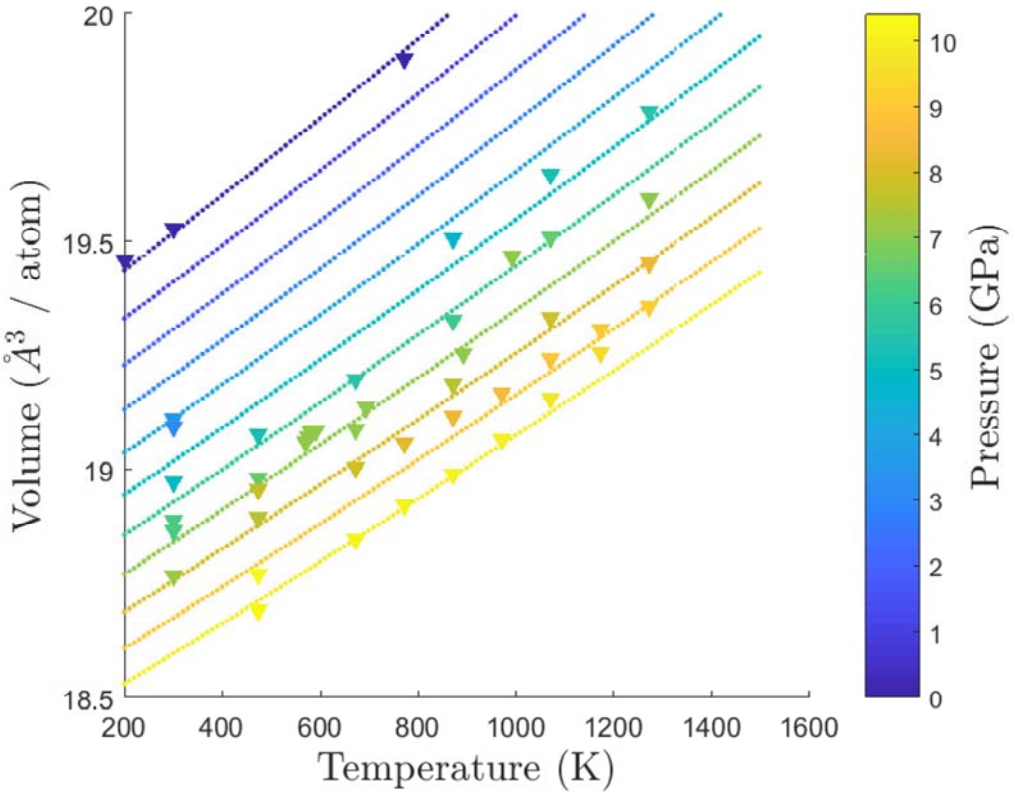

Figure 5 Refined *p*-*V*-*T* equation of state of *rs*-ZnO using our thermal expansion data (sample # 1, 0.1 MPa), and previously reported compressibility data: isobar at 7 GPa,[13] and high-pressure – high-temperature data to 10 GPa and 1270 K.[32]

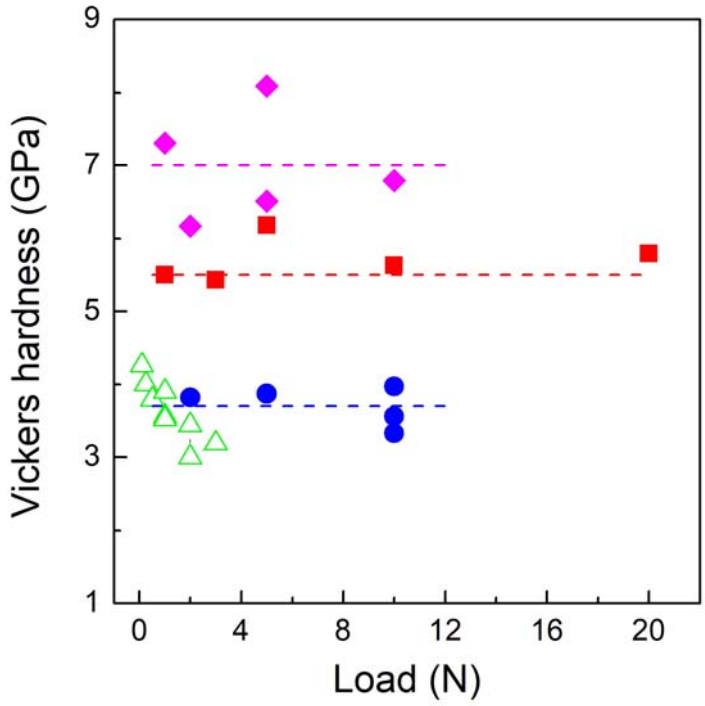

Figure 6 Vickers hardness of ZnO polymorphs: polycrystalline *w*-ZnO (green triangles); single-crystal *w*-ZnO (blue circles); nanocrystalline *rs*-ZnO synthesized from soft-chemistry nanoparticles of *w*-ZnO [4] (red squares); nanocrystalline *rs*-ZnO (sample # 1) (magenta diamonds).